




OPEN

Research on a capacitive particle analysis smoke detector

Boqiang Wang^{1,2}, Xuezheng Zhao², Yiyong Zhang^{1,2}, Zigang Song² & Zhuogang Wang²

Smoke detectors face the challenges of increasing accuracy, sensitivity, and high reliability in complex use environments to ensure the timeliness, accuracy, and reliability of very early fire detection. The improvement and innovation of the principle and algorithm for smoke particle concentration detection provide opportunities for improving the performance of the detector. This study represents a new refinement of the smoke concentration detection principle based on capacitive detection of cell structures, and detection signals are processed by a multiscale smoke particle concentration detection algorithm to calculate smoke concentration. Through experiments, it was found that the detector provides effective detection of smoke particle concentrations ranging from 0 to 10% obs/m; moreover, when the detection accuracy is greater than a certain number of parts per million (PPM), the sensitivity of the detector can reach the PPM level; furthermore, the detector can detect smoke particle concentrations higher than the PPM level accuracy even in an environment with a certain concentration of petroliferous and dust particles of different sizes.

Keywords Extreme early fire detection, Smoke concentration detection, Capacitive detection, Multiscale signal processing

Very low concentrations of smoke particles can be effectively detected during very early fire detection. This approach of capacitive particle detection method can effectively control the further development of fires and minimize losses of all kinds of fires. Unfortunately, there are greater than 100,000 cases of no alarm generation or alarm failure¹, and more than 200,000 false alarms were responded to by fire departments². These factors are expected to result in unnecessary losses, waste of firefighting resources, and declining public confidence. The fast and accurate detection of smoke particles from very quick fires is critical for avoiding losses and saving lives. It is required that the detector has a sensitivity of PPM level, and a smoke concentration measurement range of 0–20% obs/m, and power consumption should be kept under 30W.

Smoke concentration detection technology confronts the challenges of responding to the effects of interfering particles in complex environments, false alarm resistance, and adaptation. The interfering particles mainly come from airborne dust particles, oil and gas particles, and water vapor particles. The concentration of interfering particles usually ranges from 0.05 to 5% obs/m. Conventional point smoke detectors are unable to cope with harsh and intrusive environments³. Photoelectric smoke detectors are unable to distinguish between particle signals of different sizes, but the detector response speed increases when the emitting light source is a green LED⁴. Very low-concentration smoke particles (0.1% obs/m) released from very early fires can be effectively recognized by a photoelectric aspirating smoke detector, and this type of detector has achieved successful commercial application⁵. However, this approach can only partially eliminate the effect of other interfering particles through the filter and cannot distinguish the particle type. These factors significantly limit the applicability of the detector: the impact of the airflow direction on the mounting angle of the detector needs to be considered when designing the layout style of the pipeline⁶; the air sample pipeline needs to be complexly modeled in 3D to verify the reasonableness of the pipeline layout⁷; and the trajectories of smoke particles need to be identified by using computational fluid dynamics⁸. The false alarm resistance of a detector can be improved by adding a combustible gas detection module for alarm calibration⁹. A capacitive bending smoke sensor can increase its sensitivity by increasing the component contract area. However, it is still not able to distinguish between the types of particles, and false alarms can still occur¹⁰. A capacitive smoke sensor based on MEMS technology can detect smoke generated by hydrogen-containing substances during the smoldering stage. But, it is not sensitive to smoke particles by combustion of carbon-containing substances¹¹. However, this approach also affects the sensitivity of the detector to a certain extent. While very low concentrations of smoke particles generated by very early fires are effectively detected, the effective identification of particle types is still a problem. Moreover, the

¹Harbin Institute of Technology, 92 Xidazhi Street, Harbin 150006, Heilongjiang, China. ²China State Shipbuilding Corporation Limited 703 Research Institute, 35 Honghu Street, Harbin 150010, Heilongjiang, China. ✉email: 2534786721@qq.com

false alarm rate of the detector will increase, and its reliability will be greatly affected in complex environments where oil gas particles and dust particles of different sizes are present. The diameter of smoke particles usually ranges from 0.1 to 100 μm .

In this study, a structure for analyzing and detecting smoke particles based on capacitive detection element cells is designed, and particles of different sizes will form mixed signals with different amplitudes and frequencies when they pass through the detection structure. A multiscale algorithm is used to detect smoke particle concentrations by sequentially analyzing mixed signals via time–frequency domain analysis, extracting smoke particle signals, sensitizing smoke signals, and calculating smoke concentrations. On the one hand, the detector will have higher detection accuracy and sensitivity because smoke particles are detected by the newly designed capacitive detection cell. On the other hand, the detector can differentiate signal characteristics effectively between different particles through the newly designed particle detection structure and algorithm so that the reliability of the detector increases in complex environments. The sensitivity, accuracy, and reliability of the proposed method were verified through a limit concentration detection experiment, smoke concentration detection experiment, and anti-interference ability experiment, respectively.

Capacitive smoke particle detection principle and design

Capacitive particle analyzer detector structure

As shown in Fig. 1, the capacitive particle analysis structure mainly consists of a pair of capacitive particle detection plates, a gas sample sampling path, a motive air path, and a signal processing circuit. Capacitive particle detection plates consist of a fixed capacitive plate and a flexible capacitive plate for detecting the particle type. The gas sample sampling path consisted of inlet/outlet fans, an inlet/outlet gas line, and a particle detection chamber to sample the air samples. The power gas path consists of filters, a blower, and a variable diameter jet exhaust to provide the kinetic energy for the sampled air sample to collide with the flexible capacitive plate.

Particle detection principle

As shown in Fig. 2a, The signal stacker is used to accumulate the signals measured by all capacitance cells. The schematic diagram of the interface circuit is shown in Fig. 2b. smoke particles and interference particles are simultaneously inhaled into the particle detection chamber by the inlet fan. The air inhaled by the blower will be purified into clean power gas after passing through two layers of coarse and fine filters. Inhaled smoke particles and interference particles are blown by such gas to the flexible capacitive plate and collide with it. Suppose that vertical deformations of ΔL_1 and ΔL_2 are formed by a collision between interference particles and smoke particles on the flexible capacitive plate, respectively. Then, the capacitance on the capacitance cell changes as follows:

$$\begin{cases} C_{\Delta L_1} = \frac{\varepsilon \cdot A}{d - \Delta L_1} \\ C_{\Delta L_2} = \frac{\varepsilon \cdot A}{d - \Delta L_2} \end{cases} \quad (1)$$

where $C_{\Delta L_1}$ and $C_{\Delta L_2}$ are the capacitance variations generated on the impinged capacitance cell by interference particles and smoke particles, respectively; d is the distance between the fixed capacitive plate and the flexible

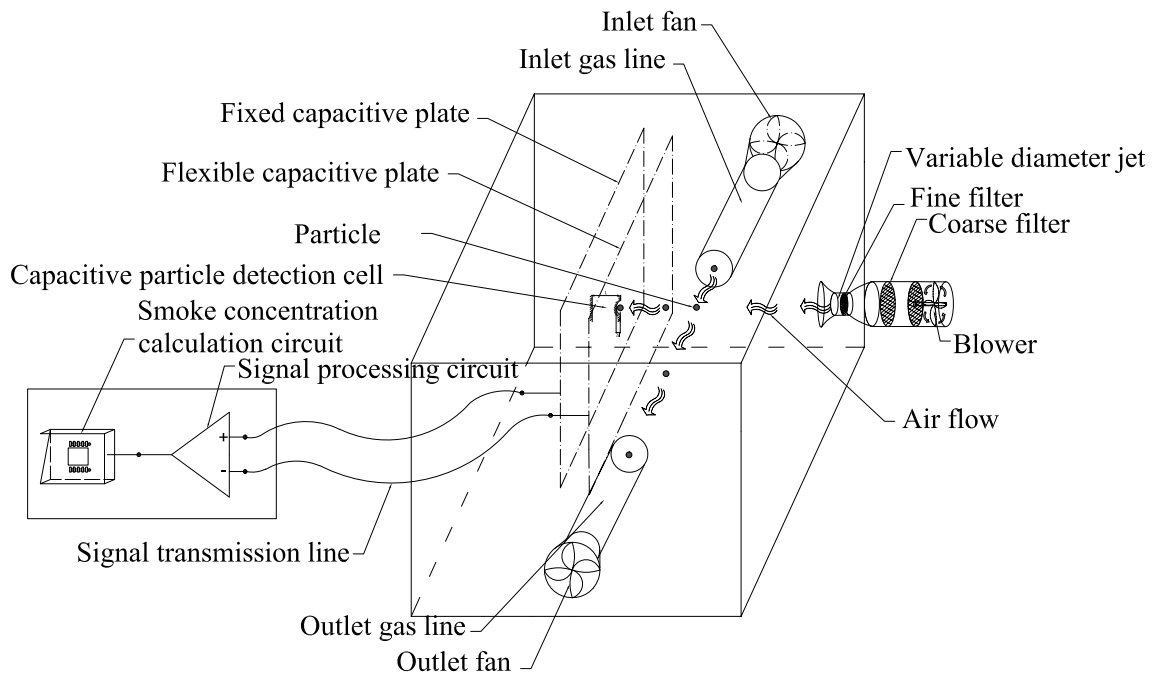
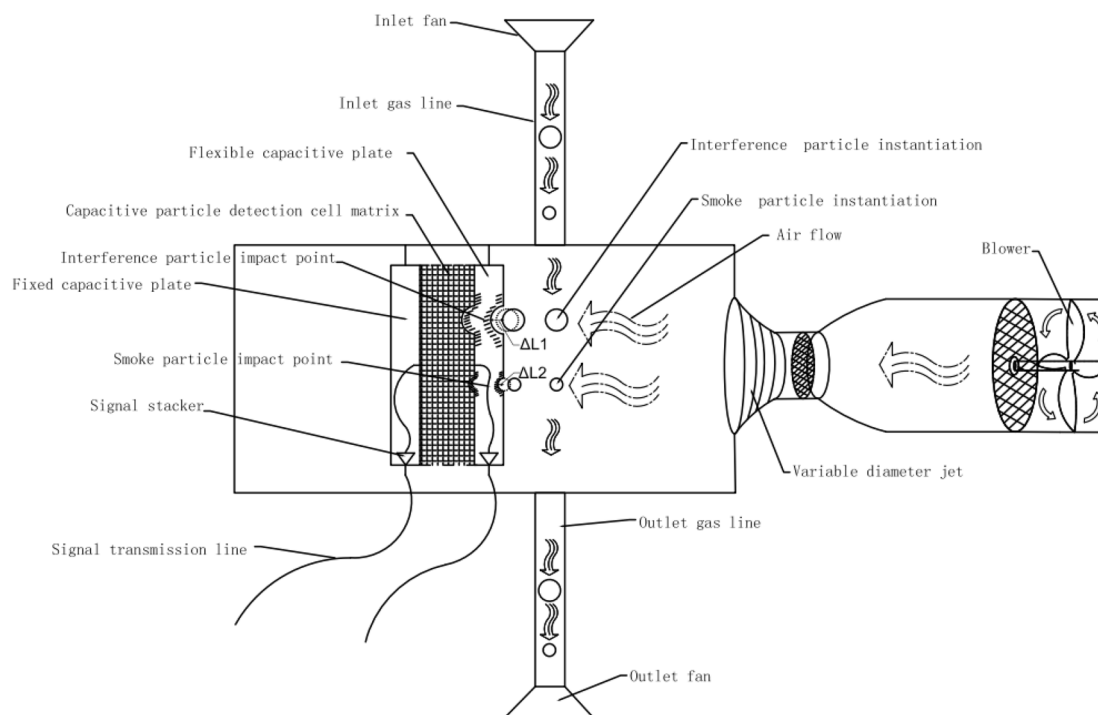
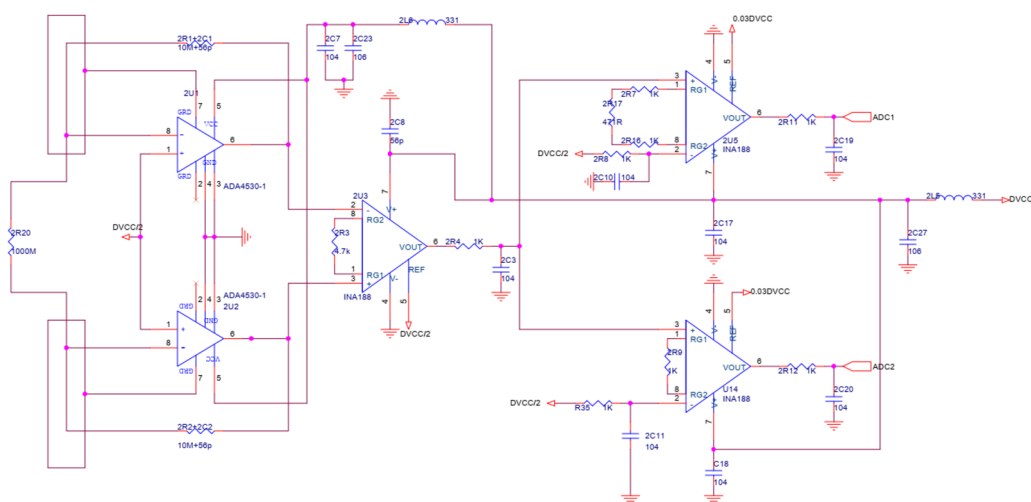


Figure 1. Capacitive particle analysis structure schematic.



(a) Schematic diagram of the capacitive cell structure



(b) Signal processing circuit

Figure 2. Particle detection schematic and signal processing circuit.

capacitive plate before the collision; and ϵ is the permittivity of the capacitor, A the relative projected area of the two capacitive plates.

A fixed DC voltage U is applied between the fixed capacitive plate and the flexible capacitive plate. A precision sampling resistor is connected in series between two signal stackers of the fixed capacitive plate and flexible capacitive plate, and the signal stacker is used to collect the electrical signal produced by capacitive cells. Induced currents flow through the sampling resistor, and a voltage is produced when the change in capacitance is caused by particle impacts on the flexible plate.

Capacitor detection cell design

The particles will only collide with the flexible plate in the normal direction. Because, the particle is only acted upon by the force in the normal direction. The normal force comes from the blower.

The vertical orientation of the capacitive cell is designed based on the dense grid medium, as shown in Fig. 3a. It mainly consists of a cell strain detection pole, a cell dielectric layer, and a fixed cell plate, and the cell strain detection pole consists of several micro detection units connected by a bus line. Eventually, the electrical signal from the microdetection unit is collected and converted by the cell signal conversion circuit. The cell dielectric layer is made of a frothy silicon-lipid mixture. The fixed-cell plate design is based on rigid structures that prevent cutting orientation movement from affecting cell detection accuracy.

As shown in Fig. 3b, the smoke particles collide with the vertically oriented strain-inducing pole of the capacitive cell under the action of the blower. Under the effect of the collision force F_n , the dense grid medium will be compressed, which will change the distance between the fixed plate and the strain-inducing pole, thus changing the capacitance value of the capacitor. The detection of smoke particles is achieved by detecting the change in electrical signals caused by changes in capacitance.

Assuming that the invariant of the cell micro detection unit is ΔL after collision by particles, it can be expressed as follows:

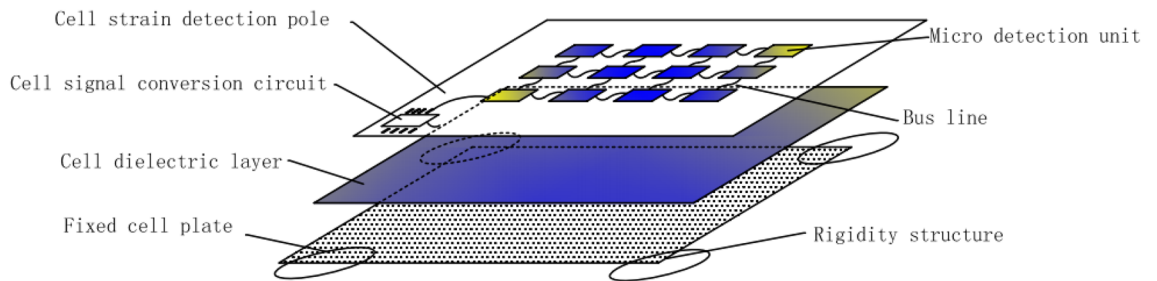
$$\Delta L = \frac{F_n d}{\rho_A E A_S} \tag{2}$$

where ρ_A is the filling rate of the cell dielectric layer, E is the elastic recovery of the cell dielectric layer, A_S is the area of the cell dielectric layer.

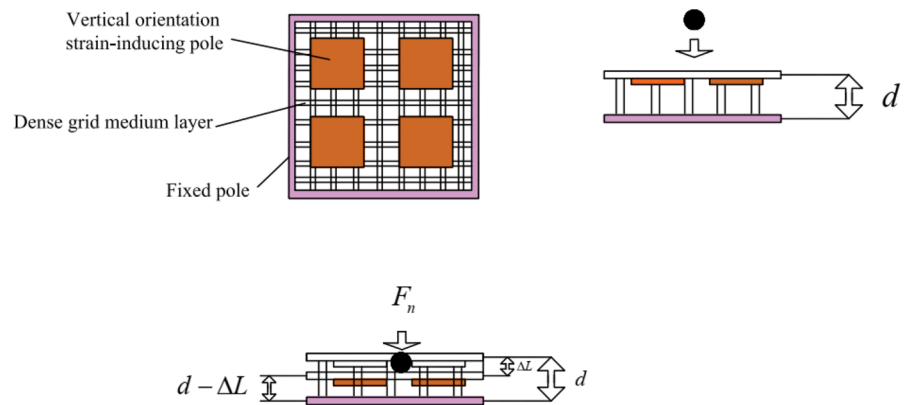
F_n can be expressed as follows:

$$F_n = \delta_i F_{fan} R_i \tag{3}$$

where δ_i is the inertia coefficient of particle type i , R_i is the diameter of particle type i , and F_{fan} is the driving force of the blower to the particles. Furthermore, capacitance variations can be obtained after the cell micro detection unit collides with particles, as shown in Eq. (4), and the sensitivity can be expressed as Eq. (5).



(a) Schematic diagram of the capacitive cell structure



(b) Schematic diagram of the capacitive smoke particle detection principle

Figure 3. Capacitive detection cell.

$$C_{\Delta L_i} = \frac{\varepsilon A_i}{d - \Delta L_i} = \frac{\varepsilon A_i}{d - \frac{\delta_i F_{fan} R_i d}{\rho_A E A_s}} \quad (4)$$

$$\frac{\partial C_{\Delta L_i}}{\partial R_i} = \frac{\varepsilon A_i \rho_A E A_s}{d(\rho_A E A_s - \delta_i F_{fan} R_i d)^2} \quad (5)$$

where A_i is the sensing electrode area of the micro detection unit and ΔL_i is the invariant of the cell micro detection unit after collision by particles. Because F_n has a much lesser impact than $\rho_A E A_s$, the impact from F_n can be ignored. At this point, the sensitivity can be expressed as

$$\frac{\partial C_{\Delta L_i}}{\partial R_i} \approx \frac{\varepsilon A_i}{d \rho_A E A_s} \quad (6)$$

A mixture of flexible body and gas gaps formed between the cell strain detection pole and the fixed cell plate. Equation (6) shows that the filling rate of the mixture on the cell dielectric layer should be reduced to improve the sensitivity.

Signal output model and algorithm model

Model of the output signal from the particle analysis structure

The capacitance changes when the flexible capacitive plate is collided by particles. Because a fixed DC voltage is applied between two plates, an alternating current will produce a change in capacitance, the amplitude of which is the superposition of all weak AC signals caused by collisions between particles (including smoke particles and interfering particles) and capacitive cells, and the signal will be output by the signal stacker between two plates. The mathematical model has been developed by assuming sinusoidal currents.

$$I_{sum} = U_0 \cdot \frac{dC_{sum}}{dt} = U_0 \cdot \left[\frac{d(C_{\Delta L_1})}{dt} + \frac{d(C_{\Delta L_2})}{dt} \right] \quad (7)$$

where I_{sum} is the total alternating current signal synthesized by the signal stacker and, U_0 is the constant voltage between capacitor's terminal, C_{sum} is the superposition of changes in the capacitance of the capacitor. The AC voltage signal is generated on the precision resistor in series between two signal stacks.

$$U_{sum} = I_{sum} * R_{samp} \quad (8)$$

where R_{samp} is the electrical resistance of the precision sampling resistor, and it has a resistance value of 10M Ω , U_{sum} is the AC voltage applied to the precision sampling resistor. A superposition of sinusoidal voltages with different frequencies and amplitudes will be formed after filtering and amplification by the signal processing circuit (as shown in Fig. 1).

$$U(t) = \sum_{R_i=R_s, R_{N_1}, R_{N_2}, \dots} A_{R_i} \cdot \sin[\omega_{R_i} \cdot t + \varphi] \quad (9)$$

where R_i is the diameter of different particles, R_s is the diameter of smoke particles to be detected, R_{N_1} , R_{N_2} , et al. are the diameters of interference particles, ω_{R_i} is the frequency of the signal produced by particles with a diameter R_i , A_{R_i} is the amplitude of the signal produced by particles with a diameter R_i , φ is the offset angle of the signal, and t is the time (Fig. 4).

Smoke concentration detection algorithm

Overall design of the multiscale smoke particle concentration detection algorithm

The signal output of the detector is in this form the superposition of signals generated by particles at different times. The weak signal needs to be amplified with the signal enhancement technique because the size of the smoke particles is tiny. These drawbacks prevent the use of a single method for signal processing from meeting the demand for smoke concentration detection. The multiscale smoke concentration detection algorithm is a combinatorial algorithm for continuous wavelet transform, smooth wavelet transform, sensitization of smoke signals, and single-frequency point concentration calculations. Therefore, the multiscale smoke concentration detection algorithm—a combination of multiple signal analysis methods—will be used for this detection, and its main steps can be divided as follows:

- First, determine the time position of the smoke particle signal in the detector output signal.
- After that, the smoke particle signal needs to be extracted.
- Subsequently, the signal after extraction is sensitized and amplified.
- Finally, the smoke concentration is calculated via single-frequency analysis.

Time–frequency analysis of signals

First, a time–spectrum analysis of the detector output signal is performed via a continuous wavelet transform along the time axis, and the moment at which the smoke particle signal appears is determined. The continuous wavelet transform of the continuous signal $f(t)$ can be expressed as follows:

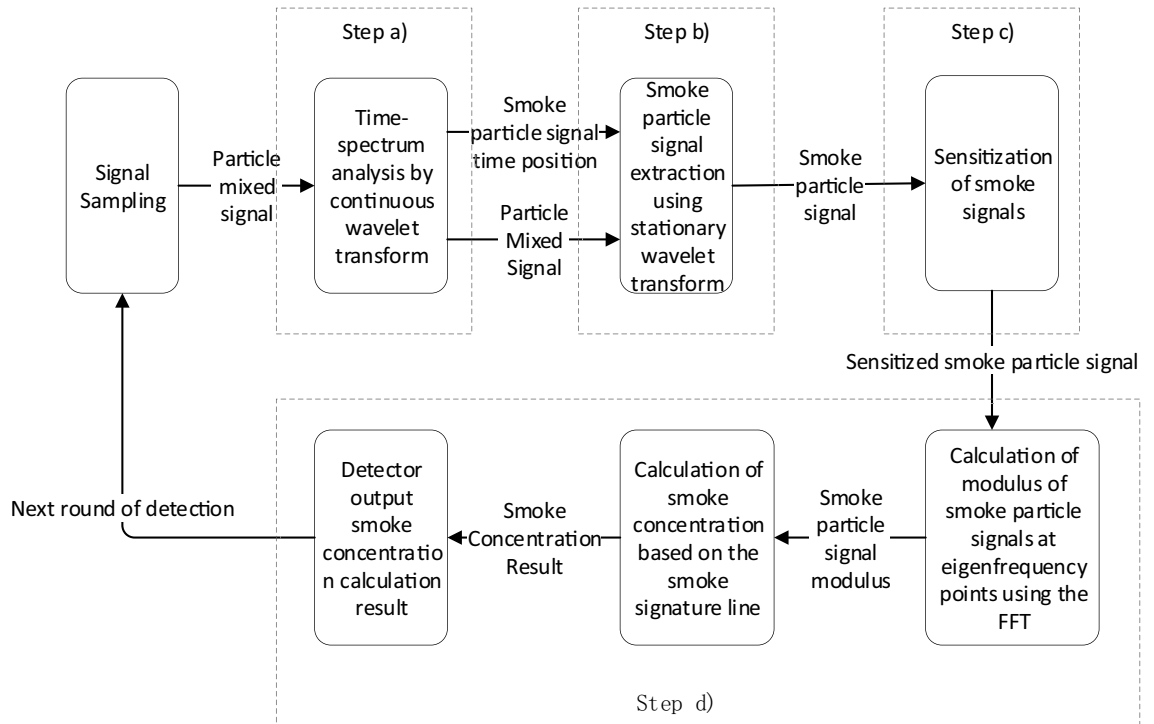


Figure 4. The flowchart of the multiscale smoke particle concentration detection algorithm.

$$WT_f(a, b) = \langle f(t), \psi_{a,b}(t) \rangle \frac{1}{\sqrt{a}} \int_{-\infty}^{+\infty} f(t) \psi^* \left(\frac{t-b}{a} \right) dt \tag{10}$$

where a is the scale parameter of the wavelet function, b is the translation parameter of the wavelet function, $\psi_{a,b}(t)$ is the wavelet basis function for parameters a and b , $\psi^*(t)$ is the conjugate function of the wavelet basis function, and $f(t)$ is the source signal function.

The relationship between the wavelet decomposition scale and signal frequency after transformation can be expressed as follows:

$$f_a = \frac{f_c f_s}{a} \tag{11}$$

where f_a is the actual signal frequency after decomposition, f_c is the center frequency of the wavelet basis function, and f_s is the sampling frequency of the signal. According to the sampling theorem, the value ranges of the scale parameter satisfy $a \in [2f_s, \infty]$ so that the value ranges of the frequency of the wavelet basis function can satisfy $f_c \in [0, f_s/2]$.

Smoke particle signal separation

In addition, the smoke particle signal is extracted from the detector output signal by a stationary wavelet transform.

In the stationary wavelet transform, the scale parameter a needs to be discretized, and the translation parameter b remains constant so that the signal after the transform has the same length as the original signal $f(t)$. The stationary wavelet transform can be obtained through discrete sampling to the scale parameter a within the binary sequence $\{2^j\}$ (where $j \in Z$).

$$SWT_f(j, b) = \langle f(t), \psi_{a,b}(t) \rangle = \frac{1}{\sqrt{2^j}} \int_{-\infty}^{+\infty} f(t) \psi^* \left(\frac{t-b}{2^j} \right) dt, j \in Z \tag{12}$$

Equation (12) shows that only the scale parameter a is discretized by the stationary wavelet transform, and the translation parameter b remains constant. In this way, the wavelet coefficients are all retained, and the length of the wavelet coefficients remains constant after each transform.

There are two ways of upsampling and downsampling at the same time so that the lengths of the signal between the original signal and the high- and low-frequency coefficients after the transform remain constant when the original signal is disintegrated by the stationary wavelet transform. This sampling mode is achieved by interpolating 2^j zeros between the two coefficients of the high-pass and low-pass filters; the high-pass and low-pass filter coefficients are stripped in this way; and the high-pass and low-pass filters in the transformation can be expressed as follows:

$$g(k) = \begin{cases} g\left(\frac{k}{2^j}\right), & k = 2^j m \\ 0, & \text{others} \end{cases} \tag{13}$$

$$h(k) = \begin{cases} h\left(\frac{k}{2^j}\right), & k = 2^j m \\ 0, & \text{others} \end{cases} \tag{14}$$

where $j, k, m \in Z$, $g(k)$ and $h(k)$ denote the unit response functions of the high-pass and low-pass filters, respectively.

Furthermore, the decomposition based on the Mallat algorithm can be obtained as follows:

$$\begin{cases} S_{j+1}(n) = \sum_{k=1}^M S_j(k)g^*(k - 2n) \\ d_{j+1}(n) = \sum_{k=1}^M d_j(k)h^*(k - 2n) \end{cases}, j = 0, 1, \dots, J \tag{15}$$

where j is the decomposition depth of the Mallat algorithm, J is the number of decompositions of the signal, n is the degree of decomposition of the signal, k is the order number of the decomposed sequence, M is the sampling point upper limit of the decomposed sequence, and $S_j(k)$ and $d_j(k)$ denote the coefficients of the high-pass and low-pass filters, respectively, at the j th signal decomposition.

The detector output signal, which includes the smoke particle signal period, is decomposed by the stationary wavelet transform based on the Mallat algorithm. Suppose that the eigenfrequency of the awaiting detection smoke particle signal is ω_{R_s} and that the eigenfrequency of the interfering particle signal is ω_{R_i} . The signal that contains only smoke particles can be acquired after i the step of stationary wavelet decomposition.

In Fig. 5, 2-s2-step decomposition is shown as an example. First, the original signal $f(t)$ is decomposed by high-pass and low-pass filters with coefficients $g_{R_{N_1}}$ and $h_{R_{N_1}}$, respectively, and the signal S_1 filters the interference caused by interference particles of size R_{N_1} and the interference signal $d_{R_{N_1}}$ generated by particles of this size. Subsequently, the signal S_1 is decomposed again by another high-pass and low-pass filter with coefficients g_{R_s} and h_{R_s} , respectively, and the signal S_{R_s} contains only the signal generated by smoke particles and the signal $d_{R_{N_2}}$ generated by interference particles of size R_{N_1} .

The relationship between the coefficients $g_{R_{N_1}}$ and $h_{R_{N_1}}$ of high-pass and low-pass filters in the first decomposition layer and the eigenfrequency $\omega_{R_{N_1}}$ of the interference signal caused by particles with size R_{N_1} can be expressed as follows:

$$g_{R_{N_1}} = \beta_{R_{N_1}} \omega_{R_{N_1}} g\left(\frac{k_{N_1}}{2^{j_{N_1}}}\right) \tag{16}$$

$$h_{R_{N_1}} = \beta_{R_{N_1}} \omega_{R_{N_1}} h\left(\frac{k_{N_1}}{2^{j_{N_1}}}\right) \tag{17}$$

where $g\left(\frac{k_{N_1}}{2^{j_{N_1}}}\right)$ and $h\left(\frac{k_{N_1}}{2^{j_{N_1}}}\right)$ are the unit response functions of the high-pass and low-pass filter decomposition depths, respectively N_1 , and $\beta_{R_{N_1}}$ is the correction coefficient for the eigenfrequency $\omega_{R_{N_1}}$.

Similarly, the relationship between the coefficients g_{R_s} and h_{R_s} of the high-pass and low-pass filters in the second decomposition layer and the eigenfrequency ω_{R_s} of the smoke signal caused by particles of size R_s can be expressed as follows:

$$g_{R_s} = \beta_{R_s} \omega_{R_s} g\left(\frac{k_{N_s}}{2^{j_{N_s}}}\right) \tag{18}$$

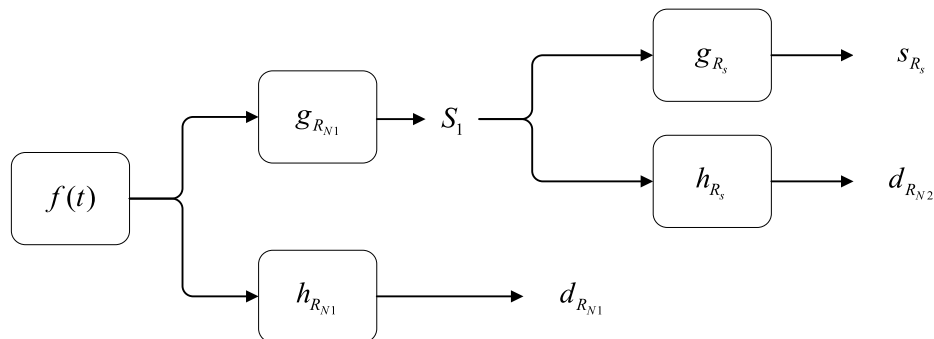


Figure 5. The signal decomposition diagram of the detector output signal by the stationary wavelet transform.

$$h_{R_S} = \beta_{R_S} \omega_{R_S} h \left(\frac{k_{N_S}}{2^{j_{N_S}}} \right) \quad (19)$$

where $g \left(\frac{k_{N_S}}{2^{j_{N_S}}} \right)$ and $h \left(\frac{k_{N_S}}{2^{j_{N_S}}} \right)$ are the unit response functions of the high-pass and low-pass filter decomposition depths, N_S respectively, and β_{R_S} is the correction coefficient for the eigenfrequency ω_{R_S} .

Signal sensitization and smoke concentration calculations

A programmable circuit, as shown in Fig. 6, is included in the signal processing circuit in Fig. 1. The circuit comprises 2 operational amplifiers (op. amps.) U28A and U29A, and a digital potentiometer U25. The very low-amplitude raw output at the sensitive element is amplified through a two-stage amplifier circuit consisting of U28A and U29A. The gain of the output signal can be adjusted by changing the tap position of the digital potentiometer U25. Finally, the processed analog signal is passed to an analog-to-digital converter (ADC). "ADC5V" is the DC 5 V power supply for the analog simulation circuit section. Capacitor C46 is used to filter the signal. Diode D3 is used to provide voltage-limited protection for the ADC signal. When the ADC voltage exceeds 12 V, diode D3 conducts to limit the ADC signal to 12 V. Electrolytic capacitors C42 and C43 are connected in reverse series to form an unpolarized capacitor of halved capacitance. This is to double the voltage rating of the capacitor.

Where $S_{R_S}^*$ is the sensitized smoke particle concentration signal and *Gain* is the signal magnification.

The fast Fourier transform (FFT) algorithm was used to calculate the modulus of a single frequency point after separation and sensitization. Near the characteristic frequency ω of the smoke particle signal, the characteristic frequency modulus M_{R_S} can be obtained.

Finally, the smoke concentration can be calculated by bringing the modulus M_{R_S} into the smoke concentration characterization line as follows:

$$Col_{R_S} = \gamma_{R_S} \times M_{R_S} + \rho_{R_S} \quad (20)$$

where Col_{R_S} is the calculated smoke concentration, γ_{R_S} is the slope of the smoke concentration characteristic line, and ρ_{R_S} is the constant of the smoke concentration characteristic line.

Experimental

Introduction of the experimental device

A smoke concentration experimental device was used to test the performance of this detector, as shown in Fig. 7a. The experiment box is the chamber that place the detector used to experiment on it. The experimental equipment is produced by Beijing Yuanhengliye Corporation, and its model number is SMK-2000. This experimental device is composed of a smoke particle generator, an interference generator, a concentration detection device, an experiment box, etc.etc. The smoke particle generator generates simulated smoke particles at different concentrations during a fire. An interference generator generates oil gas or dust particles of different sizes and concentrations in different environments. The flue mixture of the above particles was generated, and uniform particles were mixed into the experimental box when the concentration detected by the concentration detection device reached the set conditions. The concentration of various particles produced by the experimental device is measured by a sophisticated optical densitometer inside the device. The device regulates the particle concentration based on the feedback signal. As a result, the concentration accuracy of various particles generated in this device is 0.0001 PPM.

Limit concentration detection experiment

The smoke particles were separated at concentrations of 2.0 ppm and 5.0 ppm by this device, after which these particles were used to conduct a concentration limit detection experiment on the detector. The time domain signal of the smoke particle output from the detector is shown in Fig. 8, and its spectrum is shown in Fig. 9. The eigenfrequency ω_{R_S} of smoke particles can be determined to be 210 Hz.

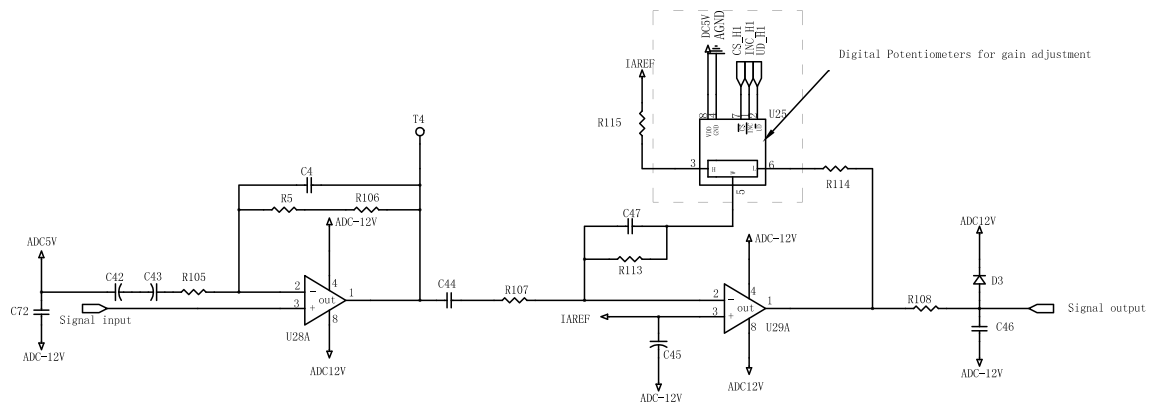
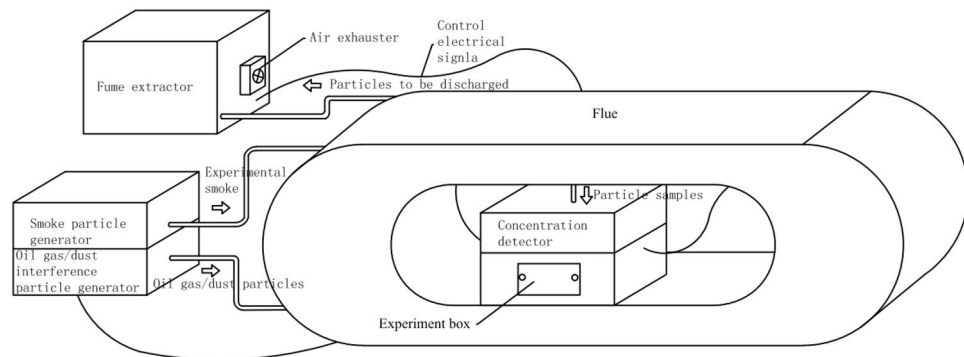
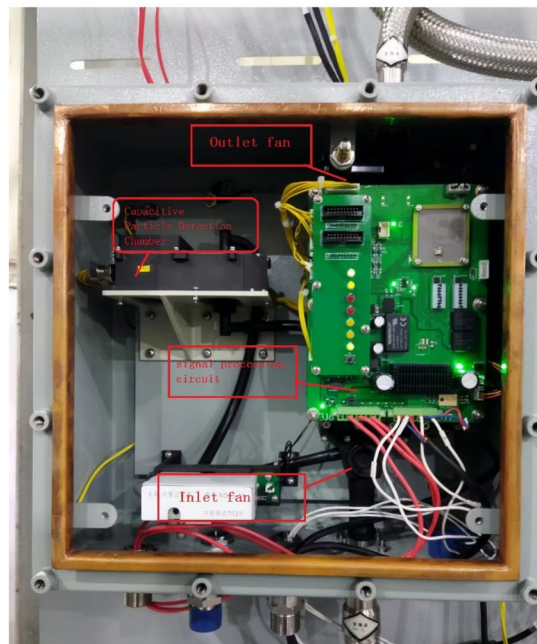


Figure 6. AC signal gain amplifier circuit schematic.



(a) Signal processing circuit



(b) Detector Physical Picture

Figure 7. Smoke concentration experimental device structure diagram and detector physical picture.

The specific calculations are shown in Table 1, and the deviations are expressed in parts-per-million (PPM) scale. The deviation is the difference between the concentration (the value shown on the concentration meter on the test set) produced by the device (shown in Fig. 7) and the actual concentration (the concentration is calculated by taking the modulus calculated by the detector at the smoke particle characteristic frequency point ω_{R_s} into Eq. (20)) measured by the detector.

As shown in Table 1, the results are 5.2PPM and 2.3PPM, with a detection deviation of less than 0.5PPM when the detector detects smoke particles at concentrations of 2PPM and 5PPM, respectively.

Smoke concentration detection experiment

Smoke particles with concentrations ranging from 0% obs/m to 10% obs/m were separated by this device, and these particles were used to conduct a concentration limit detection experiment on the detector. The time domain and signal spectrum are shown in Figs. 10 and 11, respectively, and the detection results are shown in Table 2.

Anti-interference ability experiment

Mixed particles with 6% obs/m oil gas particles, 7% obs/m large dust interference particles, 8% obs/m small dust interference particles, and 2% obs/m smoke particles were prepared, and mixed particles were pumped into the experimental box of this device for an anti-interference experiment.

The signal output from this detector is shown in Fig. 12. Subsequently, the signal of mixing with various particles is transformed by a continuous wavelet transform to obtain the time–frequency distribution, as shown

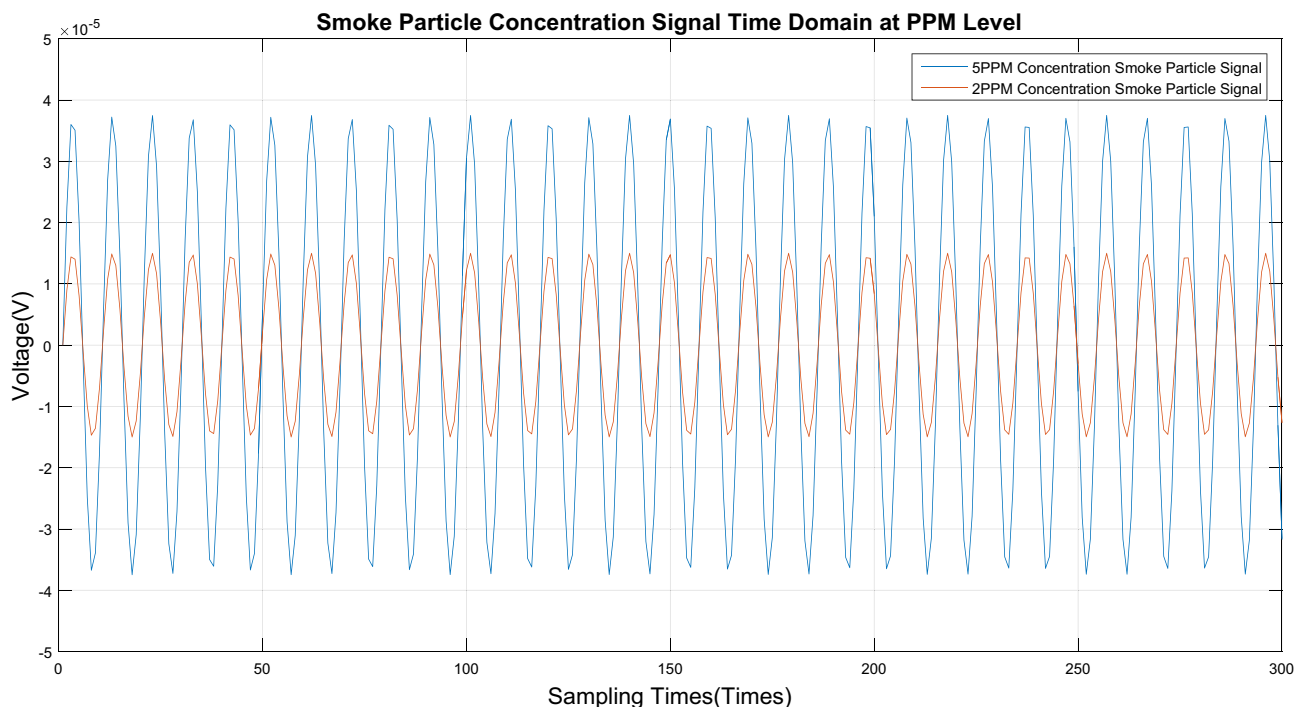


Figure 8. Time domain signal for diagram limit concentration detection.

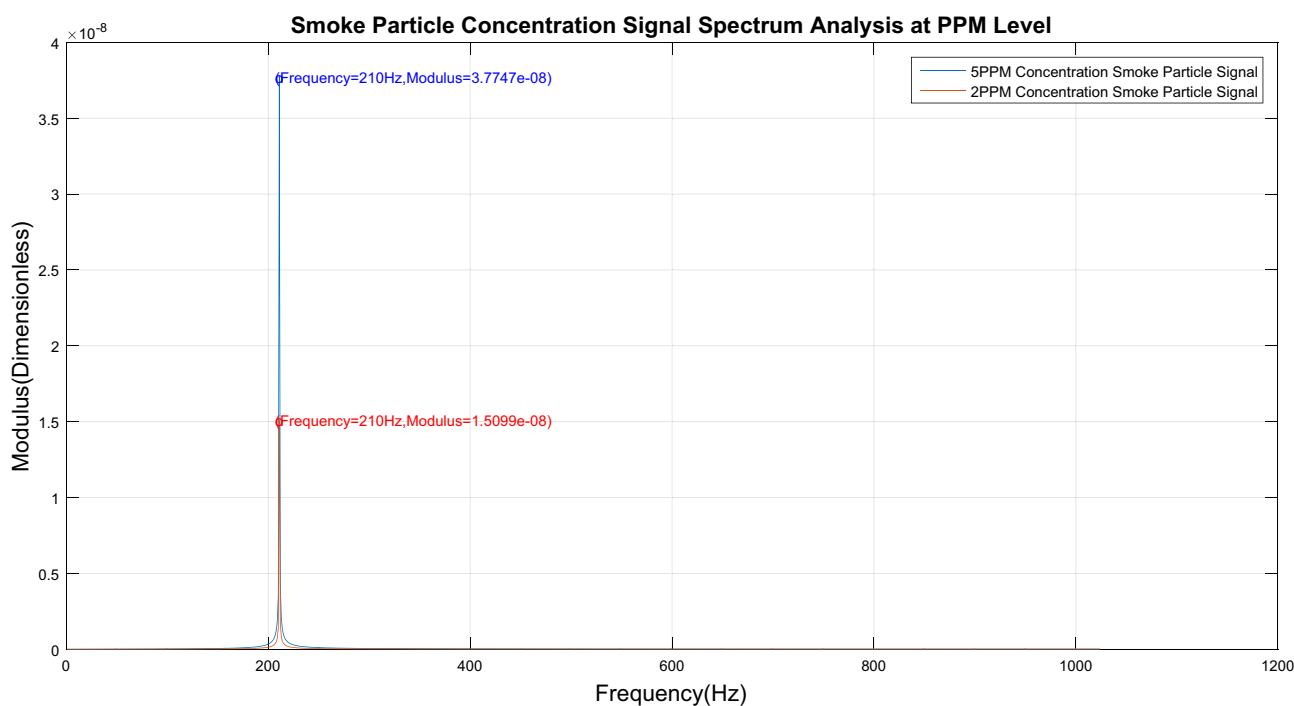


Figure 9. Limit concentration detection spectrum.

Smoke concentration (PPM)	Modulus (dimensionless)	Detection concentration (PPM)	Deviation (PPM)
2	0.000150994058	2.3	0.2
5	0.0003774835145	5.2	0.3

Table 1. Smoke concentration experiment results.

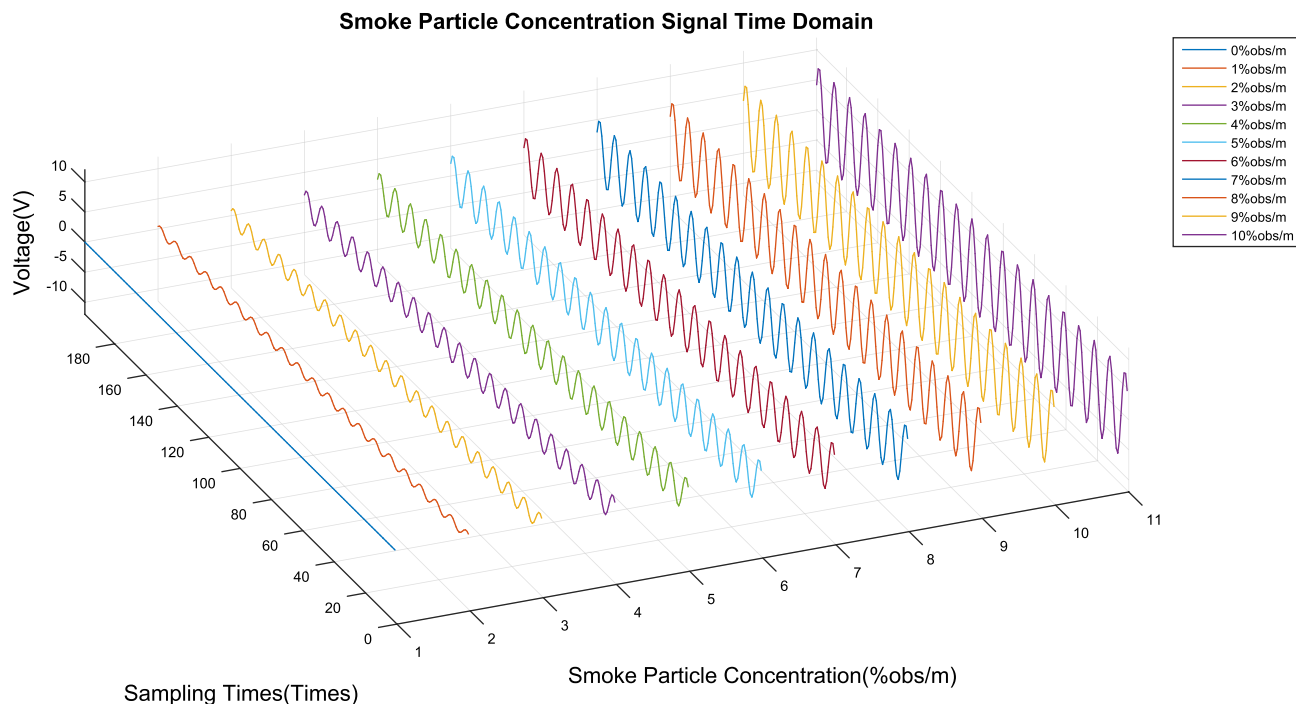


Figure 10. Time domain signal of 0–10% obs/m smoke particle concentration.

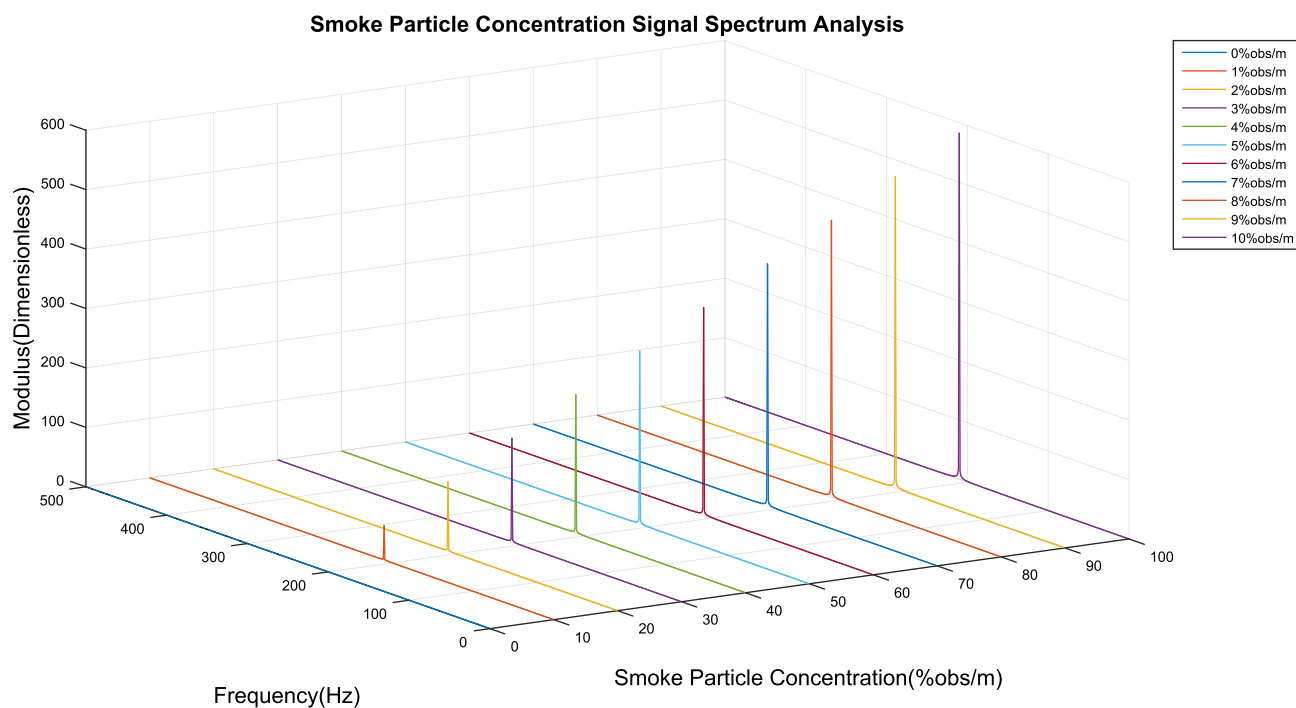


Figure 11. Spectrum of 0–10% obs/m smoke particle concentration.

in Fig. 13. From that figure, it can be seen that there are 4 main frequencies, and the signal with a frequency of 200 Hz is distributed over the whole timeline.

Furthermore, the signals generated by mixed particles are decomposed to obtain the smoke particle signal. The time domain diagrams before and after signal decomposition are shown in Fig. 14. Then, a spectral analysis of the various particle signals after decomposition was performed, as shown in Fig. 15. It is apparent from this figure that there are 4 main frequency points at 20 Hz (oil gas particle signal), 80 Hz (large dust interference particle signal), 158 Hz (small dust interference particle signal), and 210 Hz (smoke particle signal).

Finally, the smoke particle concentration was calculated, and the results are shown in Table 3. The detection concentration was 2.0000007% obs/m, and the detection accuracy was higher than that of the PPM.

Smoke concentration (%obs/m)	Modulus (dimensionless)	Detection concentration (%obs/m)	Deviation (PPM)
1	58.2667029	1.0000003	0.3
2	116.5334059	2.0000002	0.2
3	174.8001084	3.0000003	0.3
4	233.0668105	4.0000004	0.4
5	291.3335132	5.0000003	0.3
6	349.6002158	6.0000002	0.2
7	407.8669182	7.0000003	0.3
8	466.1336209	8.0000004	0.4
9	524.4003241	9.0000002	0.2
10	582.6670265	10.0000003	0.2

Table 2. Smoke concentration experiment results.

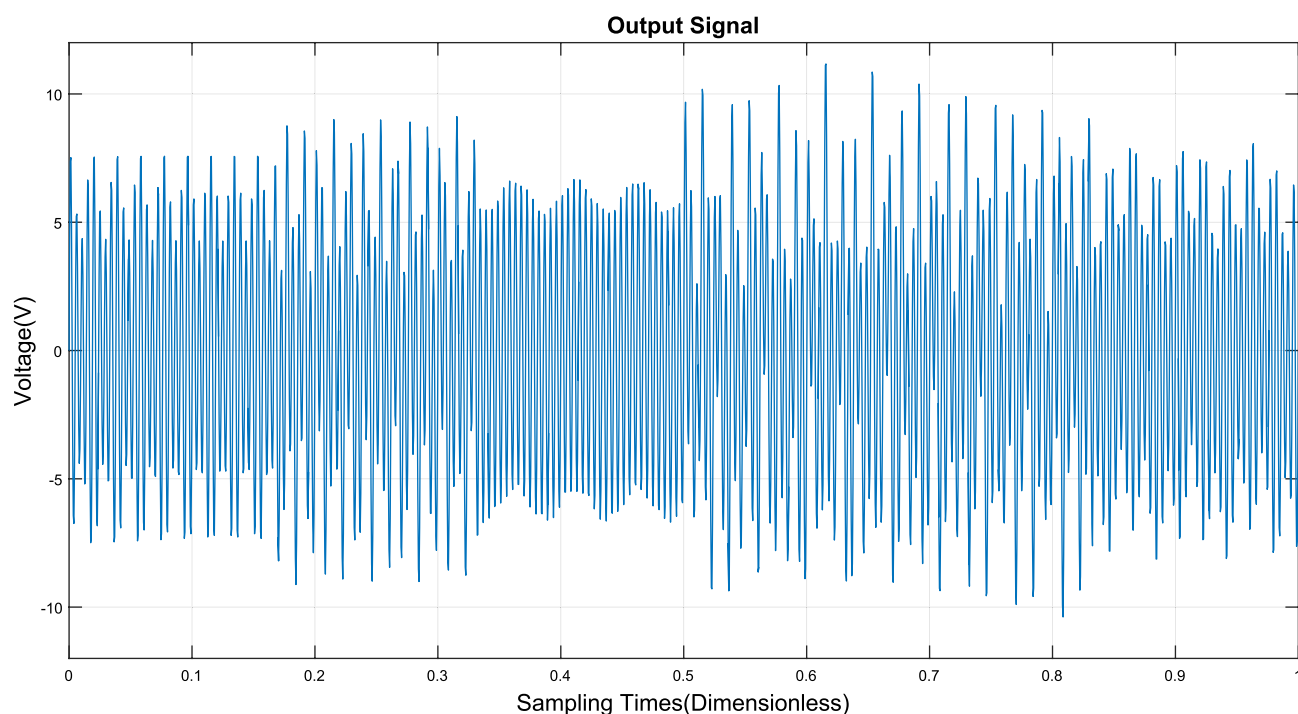


Figure 12. Interference experiment detector signal output diagram.

From the experimental results, it can be seen that the detector separates the smoke particle signals. Therefore, it can distinguish between smoke particles and other interfering particles. The detector has excellent false alarm resistance and reliability.

Comparison with previously reported methods

Compare the performance of the capacitive particle analysis smoke detector with other mainstream detectors in the industry, as shown in Table 4. The other three sensors are %obs/m level, which is significantly less accurate than the PPM level reached by the capacitive particle analysis smoke detector. The capacitive particle analysis smoke detector has a sensitivity level of PPM, which is significantly higher than the other three detectors. Only the capacitive particle analysis smoke detector can be able to recognize the different particle types. Therefore, it has higher anti-false alarm capability and reliability.

Conclusions

1. The limit of the smoke particle concentration measured by the detector reaches the PPM. The designed capacitive detection cell effectively improves the sensitivity of the detector and can measure the concentration of smoke particles effectively at the PPM level.
2. The designed detector can effectively detect smoke particles at a concentration of 0–10% obs/m, and the detection accuracy can be higher than that of the PPM. The newly designed capacitive particle analysis detec-

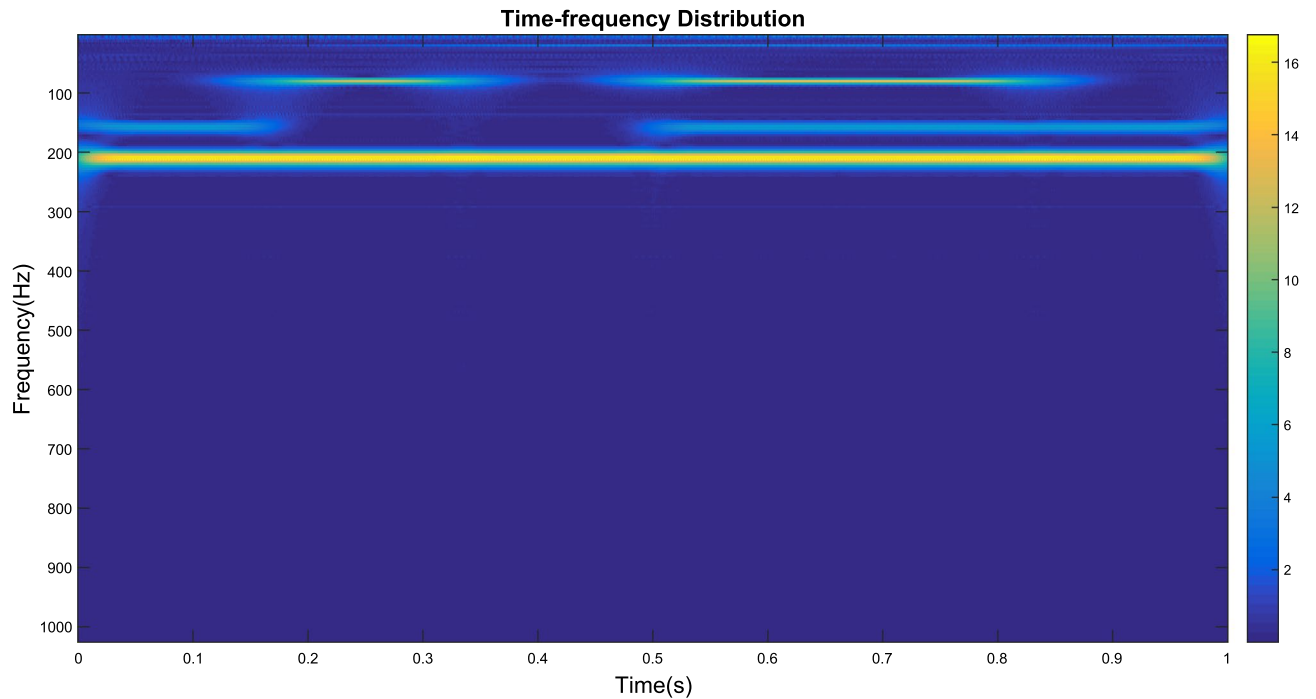


Figure 13. Time–frequency distribution.

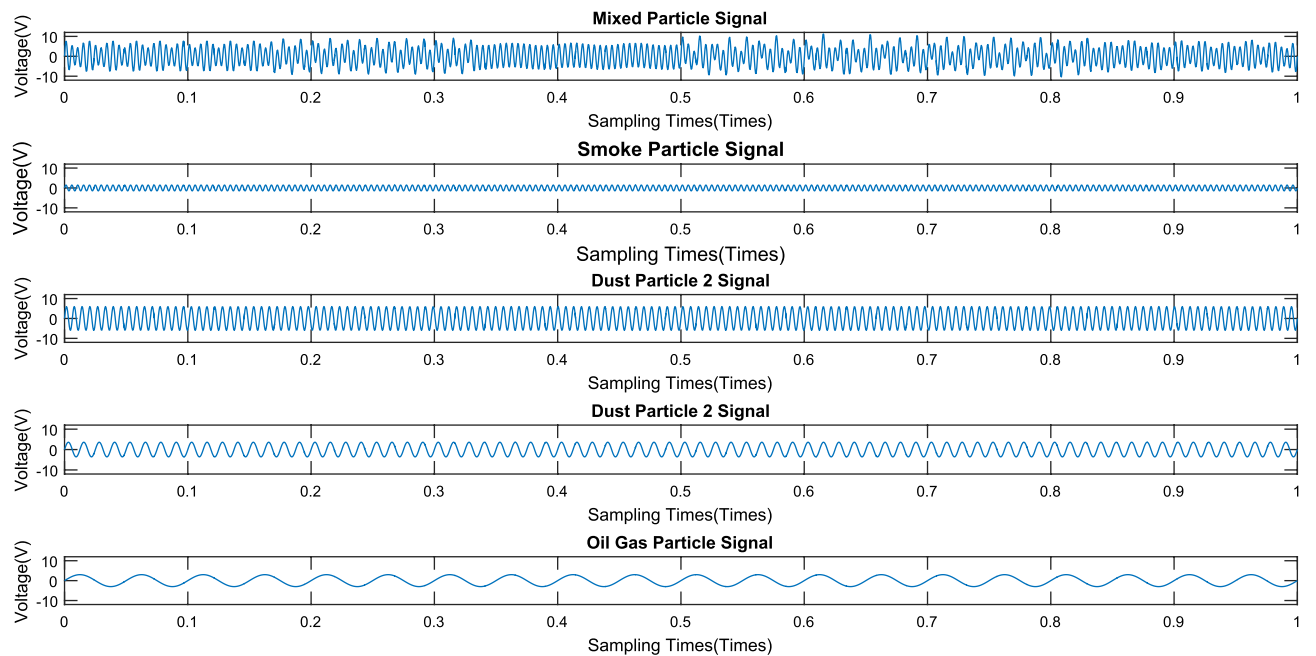


Figure 14. Signal decomposition diagram.

tor and multiscale smoke particle concentration detection algorithm can perform high-precision detection of smoke particles at various concentrations.

3. Even when there is interference from oil, gas, or dust particles, the detector can still accurately detect at a higher level than the PPM. This paper shows that capacitive particle analysis and detection structures based on capacitive detection cells combined with a multiscale smoke particle concentration detection algorithm can effectively improve the reliability of detectors to eliminate the influence of other interfering particles on detector performance in complex environments.

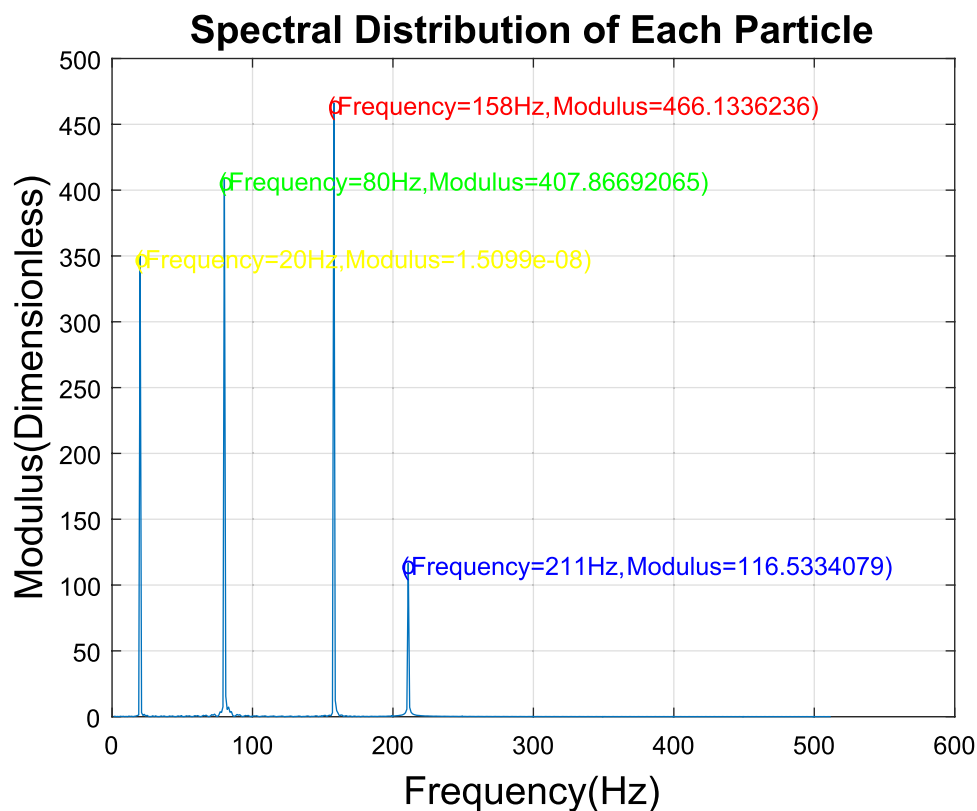


Figure 15. Spectral distribution of each particle.

Smoke concentration (%obs/m)	Modulus (dimensionless)	Detection concentration (%obs/m)	Deviation (PPM)
2	116.5334079	2.0000007	0.7

Table 3. Anti-interference ability experiment results.

Model	Manufacturer	Accuracy	Sensitivity	The ability to recognize different particle types
JTY-GD-TC9800	VESDA(UAS)	1%obs/m	0.5% obs/m	Not possess
U5014A4N13F	DET-TRONICS (UAS)	3%-5% obs/m	0.5% obs/m	Not possess
JTY-BK721	BOKANG (China)	3%-5% obs/m	1% obs/m	Not possess
The capacitive particle analysis smoke detector	HIT	2.0PPM	0.2PPM	Possess

Table 4. Comparison of detector performance.

Data availability

All data generated or analysed during this study are included in this published article.

Received: 12 January 2024; Accepted: 16 May 2024

Published online: 17 May 2024

References

- Sharma, V., Varma, A. S., Singh, A., *et al.* A critical review on the application and problems caused by false alarms. In *Intelligent Communication, Control, and Devices: Proceedings of ICICCD 2017*, 371–380 (2018).
- He, X. *et al.* Smart fire alarm systems for rapid early fire warning: Advances and challenges. *Chem. Eng. J.* **450**, 137927 (2022).
- Liu, F. *et al.* Application of aspirating smoke detectors at the fire earliest stage. *Procedia Eng.* **52**, 671–675 (2013).

4. Wei, M. C., Lin, B. R., Lin, Y. Y., *et al.* Experimental study on effects of light source and different smoke characteristics on signal intensity of photoelectric smoke detectors. In *2021 IEEE 3rd Eurasia Conference on IOT, Communication and Engineering (ECICE)*. IEEE, 518–522 (2021).
5. Johnson, P. *et al.* Very early smoke detection apparatus (VESDA), David Packham, John Petersen, Martin Cole: 2017 DiNenno Prize. *Fire Sci. Rev.* **6**(1), 1–12 (2017).
6. Lin, C. P., & Shu, C. M. Safety management on fire emergency response by VESDA applications at semiconductor plants. In *2008 IEEE International Conference on Systems, Man and Cybernetics*. IEEE, 2443–2447 (2008).
7. Višak, T. *et al.* Multi objective optimization of aspirating smoke detector sampling pipeline. *Optim. Eng.* **22**, 121–140 (2021).
8. Hu, S. C. & Chen, C. C. Locating the very early smoke detector apparatus (VESDA) in vertical laminar clean rooms according to the trajectories of smoke particles. *Build. Environ.* **42**(1), 366–371 (2007).
9. Krüll, W. *et al.* Early forest fire detection and verification using optical smoke, gas and microwave sensors. *Procedia Eng.* **45**, 584–594 (2012).
10. Maguire, G. *et al.* Smoking cessation system for preemptive smoking detection. *IEEE Internet Things J.* **9**(5), 3204–3214 (2021).
11. Hayashi, Y., Akimoto, Y., Hiramatsu, N., *et al.* Smoldering fire detection using low-power capacitive MEMS hydrogen sensor for future fire alarm. In *2021 21st International Conference on Solid-State Sensors, Actuators and Microsystems (Transducers)*. IEEE, 267–270 (2021).

Author contributions

Conceptualization, methodology, software, validation, formal analysis, writing, Boqiang Wang.; Experiment, Xuezheng Zhao, Yiyong Zhang, Zhuogang Wang and Zigang Song.

Competing interests

The authors declare no competing interests.

Additional information

Correspondence and requests for materials should be addressed to B.W.

Reprints and permissions information is available at www.nature.com/reprints.

Publisher's note Springer Nature remains neutral with regard to jurisdictional claims in published maps and institutional affiliations.



Open Access This article is licensed under a Creative Commons Attribution 4.0 International License, which permits use, sharing, adaptation, distribution and reproduction in any medium or format, as long as you give appropriate credit to the original author(s) and the source, provide a link to the Creative Commons licence, and indicate if changes were made. The images or other third party material in this article are included in the article's Creative Commons licence, unless indicated otherwise in a credit line to the material. If material is not included in the article's Creative Commons licence and your intended use is not permitted by statutory regulation or exceeds the permitted use, you will need to obtain permission directly from the copyright holder. To view a copy of this licence, visit <http://creativecommons.org/licenses/by/4.0/>.

© The Author(s) 2024